Fluids with quenched disorder: Scaling of the free energy barrier near critical points

T. Fischer and R. L. C. Vink

Institute of Theoretical Physics, Georg-August-Universität Göttingen, Friedrich-Hund-Platz 1, D-37077 Göttingen, Germany

Abstract. In the context of Monte Carlo simulations, the analysis of the probability distribution $P_L(m)$ of the order parameter m, as obtained in simulation boxes of finite linear extension L, allows for an easy estimation of the location of the critical point and the critical exponents. For Ising-like systems without quenched disorder, $P_L(m)$ becomes scale invariant at the critical point, where it assumes a characteristic bimodal shape featuring two overlapping peaks. In particular, the ratio between the value of $P_L(m)$ at the peaks ($P_{L,\max}$) and the value at the minimum in-between ($P_{L,\min}$) becomes L-independent at criticality. However, for Ising-like systems with quenched random fields, we argue that instead $\Delta F_L := \ln\left(P_{L,\max}/P_{L,\min}\right) \propto L^\theta$ should be observed, where $\theta > 0$ is the "violation of hyperscaling" exponent. Since θ is substantially non-zero, the scaling of ΔF_L with system size should be easily detectable in simulations. For two fluid models with quenched disorder, ΔF_L versus L was measured, and the expected scaling was confirmed. This provides further evidence that fluids with quenched disorder belong to the universality class of the random-field Ising model.

1. Introduction

It was postulated by de Gennes that liquid-gas type transitions in fluids confined to quenched random porous media belong to the universality class of the random field Ising model (RFIM) [1]. The unambiguous experimental verification of this conjecture remains elusive to this day [2], but there is growing numerical evidence from computer simulations [3–5] of quenched-annealed mixtures [6]. In quenched-annealed mixtures, a fluid of mobile particles is confined to a configuration of immobile (quenched) particles. The quenched particles induce a random field provided (1) their positions are sufficiently random and (2) they display a preferred affinity to one of the phases formed by the mobile particles. When either one of these conditions is not met, the conjecture of de Gennes does not apply [2, 7].

Computer simulations of quenched-annealed mixtures remain complicated. One problem is that for systems exhibiting quenched disorder an additional average over many samples drawn from the distribution characterizing the disorder needs to be taken. In addition to the thermal averaging, a disorder averaging over the different samples must be taken, and hence the computational effort is orders of magnitudes larger. The convergence of disorder averaged quantities with the number of samples is typically slow (random field systems at criticality do not self average [8–13]) and so the disorder averaging must comprise many samples. A second problem is that the critical exponents of the three-dimensional RFIM are not known very precisely. In particular, estimates for the correlation length exponent ν range from 1.1 to 2.25 [14]. Due to the large uncertainty in ν, standard finite size scaling (FSS) of simulation data is problematic. The only critical exponent of the RFIM on which there is some consensus, is the "violation of hyperscaling" exponent θ. In pure systems, meaning systems without quenched disorder, it holds that $\theta = 0$, but in the RFIM $\theta \sim 1.5$, i.e. distinctly non-zero. In order to detect RFIM universality, it follows that FSS of a quantity "somehow involving" the violation of hyperscaling exponent θ is a promising approach. In this paper, we present one such strategy, based on the free energy cost of interface formation. In the RFIM at its critical point, the barrier diverges with the system size as

$$\Delta F_L \propto L^\theta, \tag{1}$$

where L is the lateral extension of the simulation box [5]. In the pure Ising model where $\theta = 0$, ΔF_L is L-independent at criticality [5, 15, 16]. Since θ is large in the RFIM, the divergence of ΔF_L should be easily detectable in random field systems.

The outline of this paper is as follows. We first describe how the scaling of the free energy barrier at criticality can be derived and exploited in the context of FSS. We then illustrate the approach for the RFIM, the Widom-Rowlinson (WR) model [17] with quenched obstacles, and the Asakura-Oosawa (AO) model [18, 19] of colloid-polymer mixtures inside a porous medium. In all cases $\theta > 0$ is observed, but the precise value varies. For the RFIM and WR mixture $\theta \sim 1.5$ is obtained, while colloid-polymer mixtures yield a somewhat lower value $\theta \sim 1.0$; possible origins for this discrepancy are discussed in Section 4.

2. Finite size scaling of the interface free energy

2.1. theoretical background

We assume that the RFIM in $d = 3$ dimensions undergoes a continuous phase transition, at critical temperature T_c, from a disordered phase at high temperature, to an ordered phase with finite magnetization at low temperature. The existence of a transition at nonzero temperature was controversial until a proof for the existence of a spontaneous magnetization settled this issue [20]; rigorous results on the order of the transition remain elusive, but numerical studies [21, 22] indicate that the transition is continuous. Following convention, we define the relative distance from the critical point as

$$t := T/T_c - 1. \tag{2}$$

In the vicinity of the critical point, $t = 0$, the correlation length diverges as a power law

$$\xi \propto |t|^{-\nu}, \tag{3}$$

while in the ordered phase a finite interfacial tension (excess free energy per unit of interface) develops

$$\sigma \propto |t|^{2-\alpha-\nu} \quad (t < 0), \tag{4}$$

where α is the critical exponent of the specific heat. Near the critical point, the correlation length is the only relevant length scale, and so a simple dimensional argument implies that the total interface free energy must scale as

$$\Delta F_\xi \propto \sigma\, \xi^{d-1} \propto |t|^{2-\alpha-\nu} \xi^{d-1} \propto \xi^{(\alpha+d\nu-2)/\nu}, \tag{5}$$

where in the last step t was eliminated using Eq. (3). If we now use the FSS "Ansatz" $\xi \propto L$, the above equation reduces to

$$\Delta F_L \propto L^{(\alpha+d\nu-2)/\nu}, \tag{6}$$

which describes the scaling of the interface excess free energy in a finite simulation box of lateral extension L in the vicinity of T_c. This equation applies to both the pure Ising model and the RFIM. The hallmark of RFIM universality is the modified hyperscaling relation [23–25]

$$2 - \alpha = \nu(d - \theta), \tag{7}$$

which upon substitution in Eq. (6) yields

$$\Delta F_L \propto L^\theta, \tag{8}$$

and so we have derived Eq. (1). In the pure Ising model $\theta = 0$, in which case the barrier does not depend on L at the critical point (as is well known [15]). In the RFIM $\theta \sim 1.5$, implying a strong divergence with system size.

2.2. order parameter distributions

We now explain how the barrier ΔF_L is measured in computer simulations of liquid-gas type transitions. For simplicity, we first consider a single component fluid in the absence of quenched disorder. The key quantity is the order parameter distribution (OPD)

$$P_L(\rho|T,\mu) \qquad \text{(single component fluid)}, \tag{9}$$

defined as the probability to observe a state with particle density ρ. The OPD is measured in the grand canonical ensemble, at fixed temperature T and chemical potential μ, using a periodic $L \times L \times L$ simulation box [26, 27]. Below the critical temperature T_c and at the coexistence chemical potential μ_{cx}, the OPD becomes bimodal; the peak at low (high) density corresponds to the gas (liquid) phase. The coexistence chemical potential is obtained by maximizing the derivative of the average density with respect to μ

$$\mu_{cx} : \partial\langle\rho\rangle/\partial\mu \to \max, \tag{10}$$

with $\langle\rho\rangle = \int \rho\, P_L(\rho|T,\mu)\, d\rho$. Note that other choices to define μ_{cx} are possible also [28], most notably the "equal-weight" rule [29], but Eq. (10) has the advantage that it remains well-defined also when the peaks in the OPD overlap. The free energy barrier ΔF_L is encoded in the logarithm of the OPD: it corresponds to the average peak height of $\ln P_L(\rho)$, measured from the minimum "in-between" the peaks [30].

In athermal binary mixtures with mobile species A and B (but still without disorder), the analogue of Eq. (9) becomes

$$P_L(\rho_A|z_A,z_B) \qquad \text{(athermal binary mixture)}, \tag{11}$$

where ρ_A is the density of the A particles, and where z_A and z_B are the fugacities of the A and B particles, respectively. By athermal we mean that the particle interactions are either hard-core or ideal, as is the case in the WR and AO models. Those mixtures correspond to a single component fluid if one identifies $\rho \leftrightarrow \rho_A$, $T \leftrightarrow 1/z_B$, and $\mu \leftrightarrow \ln z_A$. The transition between a "gas phase" with low ρ_A and a "liquid phase" with high ρ_A is now driven by the fugacities. It occurs on the coexistence curve $z_A = z_{cx}(z_B)$, provided the fugacity of the B particles exceeds the critical fugacity $z_B > z_c$. On the coexistence curve, which again can be found using Eq. (10), the OPD becomes bimodal and allows the extraction of a free energy barrier ΔF_L, see Fig. 1(a).

We now consider an athermal binary mixture in the presence of quenched disorder. We thus have mobile particles A and B as before, but also quenched obstacles which are distributed at random locations at the start of each simulation after which they remain frozen. The A and B particles then diffuse through the quenched environment. From the set of all possible configurations of quenched disorder, we consider a finite number of N configurations, and for each of them the OPD is measured. Instead of a single OPD as in Eq. (11), we thus have a set of distributions

$$P_{L,i}(\rho_A|z_B,z_A), \tag{12}$$

where $i = 1,\ldots,N$ labels the different configurations. Even though we are interested in the OPDs for different fugacities, it is sufficient to simulate only a few combinations: having simulated a system at some (z_A, z_B), the OPDs for nearby fugacities can be obtained via histogram reweighting [31]. To facilitate an efficient storage of the data, the approach of [3, 5] is used. Meaningful results around the critical point require $N \sim 10^{3-4}$, so the computational effort is much larger compared to the pure systems.

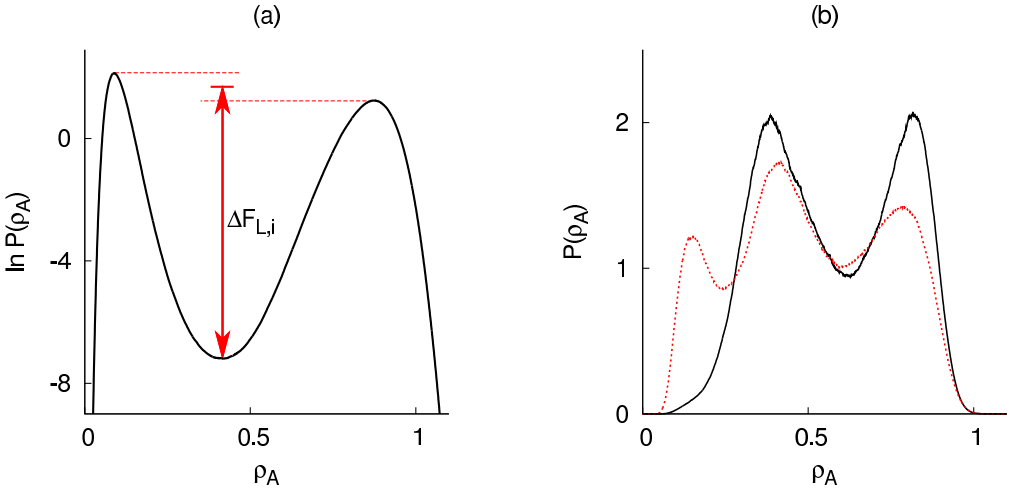

Figure 1. (a) Example OPD for the WR mixture (with quenched obstacles) obtained for $z_B = 1.2$, $L = 12$, and z_A chosen according to Eq. (10). Note that the natural logarithm of the distribution is shown. The barrier $\Delta F_{L,i}$ corresponds to the average peak height (vertical arrow). (b) Example of two "problematic" OPDs, again for $z_B = 1.2$, $L = 12$, and z_A tuned according to Eq. (10). These distributions feature a peak at intermediate density, which does not correspond to a gas or liquid phase. The intermediate peak either replaces the gas or liquid peak, in which case the resulting distribution remains bimodal (solid curve), or it appears as a third peak (dashed curve). A free energy barrier corresponding to coexisting gas and liquid phases cannot be extracted from these distributions.

2.3. extracting the free energy barrier

To obtain the quenched-averaged free energy barrier, we extract the free energy barrier $\Delta F_{L,i}$ for each configuration separately, as in Fig. 1(a), and then average these values. To be precise: for a given z_B, each OPD is tuned to coexistence via Eq. (10), which implies that $z_{\rm cx}$ varies between disorder configurations [3, 5]. By tuning the distributions separately, we ensure that the majority of them become bimodal, such that a barrier can indeed be "read-off". From the individual barriers, the quenched-averaged barrier is obtained as a simple average:

$$\Delta F_L = (1/N) \sum_{i=1}^{N} \Delta F_{L,i}. \tag{13}$$

The finite number of disorder configurations used in calculating the barrier gives rise to a statistical deviation

$$u_L^2 := \frac{1}{\sqrt{N(N-1)}} \sum_{i=1}^{N} (\Delta F_{L,i} - \Delta F_L)^2 \tag{14}$$

which represents the expected deviation of our result from the result we were to obtain for $N \to \infty$.

In practice, obtaining the barrier $\Delta F_{L,i}$ can be problematic. For some disorder configurations, the OPD does not feature a clear liquid and gas peak under the criterion of Eq. (10). In these cases, an intermediate peak is seen, at a density roughly between that of the liquid and gas. This extra peak can occur as a replacement for either

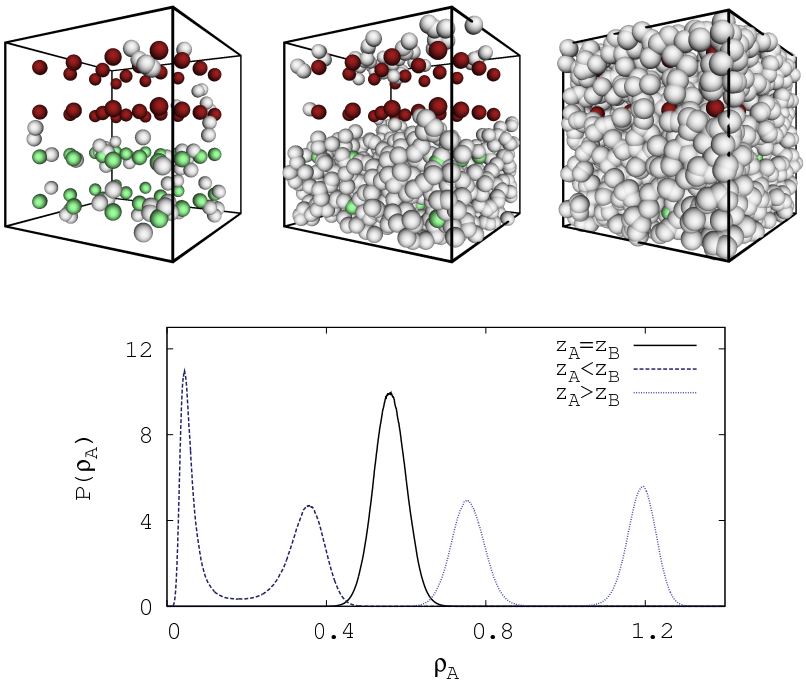

Figure 2. Illustration of how the "problematic" OPDs in Fig. 1(b) might arise. We provide data for the WR model (particle species A and B) with a configuration of quenched obstacles explicitly tailored to feature a peak in the OPD at intermediate density. Instead of distributing the obstacles randomly, they are placed on a regular grid; the obstacles in the lower half of the grid favor A particles, those in the upper half B particles. This configuration yields three stable states, depicted in the snapshots of the upper row, which were obtained for $z_B = 1.3$ and $L = 12$. For clarity, only the A particles and obstacles are shown. The first state is a homogeneous gas phase, characterized by a low density of A particles (left frame). The second is an *inhomogeneous* state, with a high (low) density of A particles in the lower (upper) half of the box (center frame). The third is a homogeneous liquid phase, characterized by a high density of A particles (right frame). The graph shows the corresponding OPD at three values of z_A. For $z_A = z_B$, a single peak is observed at intermediate density (solid curve); for $z_A < z_B$, a bimodal distribution is obtained with the second peak appearing at low density (dashed curve); for $z_A > z_B$, a bimodal distribution is also obtained but with the second peak appearing at high density (dotted curve).

the liquid or gas peak, or as an additional third peak (Fig. 1(b)). The existence of these "problematic" distributions is due to cavities formed by the obstacles. In some disorder configurations, the obstacles create large regions with a local preference for either A or B particles. One can easily show that such regions induce an intermediate peak (Fig. 2). We emphasize that around the critical point such problematic distributions are scarce in the full ensemble of disorder configurations (although modified hyperscaling does allow a finite fraction of them [5]).

2.4. analysis of finite-size effects: scaling plots

Near the critical point, we expect ΔF_L to scale according to Eq. (1). Following standard FSS practice [32, 33], we test Eq. (1) using scaling plots. That is, we plot $y_L := L^{-\theta}\Delta F_L$ versus $\tau := tL^{1/\nu}$, t given by Eq. (2). Then, if the correct values for θ, ν, and T_c are used, the curves $y_L(\tau)$ for different system sizes L should collapse on top of each other. The practical difficulty with this method is assessing the quality of the collapse: seemingly good data collapses are obtained over a range of parameter values, and simple "eye gauging" becomes unreliable. To obtain the parameters of best collapse, as well as a measure of the reliability of the results, a numerical procedure was therefore used.

Given a candidate tuple $(\theta, \nu, T_\mathrm{c})$, Eq. (14) directly yields the statistical uncertainty in $y_L(\tau)$, namely $\delta y_L(\tau) = L^{-\theta}u_L$. We average $\delta y_L(\tau)$ over the different system sizes to obtain the typical statistical uncertainty $u(\tau)$ of the curves at value τ. For a given τ, the curves $y_L(\tau)$ for the different system sizes spread around some average value with a root-mean-square width $\sigma(\tau)$. We then compare $\sigma(\tau)$ to the typical statistical uncertainty $u(\tau)$ via the ratio $\sigma(\tau)/u(\tau)$. This ratio measures how strong the curves differ compared to the random scatter induced by the finite number N of obstacle configurations. To assess the quality of the collapse, we then compute the average of the ratio over some region of τ around the critical point

$$R(\theta, \nu, T_c) := \frac{1}{\tau_1 - \tau_0} \int_{\tau_0}^{\tau_1} \frac{\sigma(\tau)}{u(\tau)}\, d\tau. \tag{15}$$

Values $R < 1$ are interpreted as fully consistent with a perfect collapse of the curves, while $R > 1$ is considered less-consistent. The integration range is chosen as large as possible, but small enough to stay within the critical region. We used $\tau_0 = -0.2 \cdot 10^{-1/\nu}$ and $\tau_1 = 0.2 \cdot 10^{-1/\nu}$, which assumes a typical system size $L \sim 10$, and restricts the temperature range to $|t| < 0.2$.

3. Results

3.1. RFIM

To provide a benchmark point for our analysis, we first apply our scaling test to data for the RFIM model. These data were taken from our previous work [5], and obtained for the RFIM in three dimensions using a random field drawn from a Gaussian distribution. The total number of disorder configurations per system size equals $N \sim 10^4$. For system sizes $L = 8$, 10, 14 and 16, we examine $R(\theta, \nu, T_c)$ in the plane of critical exponents (θ, ν). For each point in the plane, the critical temperature T_c is tuned such that $R(\theta, \nu, T_\mathrm{c})$ is minimized; the value at the minimum is denoted $R_\mathrm{min}(\theta, \nu)$. The results are collected in Fig. 3 as contours. The region where $R_\mathrm{min}(\theta, \nu) \leq 1$, i.e. where the collapse is fully consistent, agrees with the expected value $\theta \sim 1.5$. Also of interest is that the region of good collapse features a tail extending toward the pure 3D Ising values ($\theta = 0, \nu \sim 0.63$) [34]. The cause of this tail is not entirely clear, but we suspect it is due to crossover effects [35]. However, at the pure Ising values, the deviation between the curves y_L exceeds the statistical fluctuation due to the finite number of disorder configurations by a factor of more than three. We conclude that the pure Ising exponents are effectively excluded by our analysis. Note that $\theta = d - 1 = 2$, i.e. the "exponent" one would observe below the critical temperature (where the transition is first-order) is also excluded.

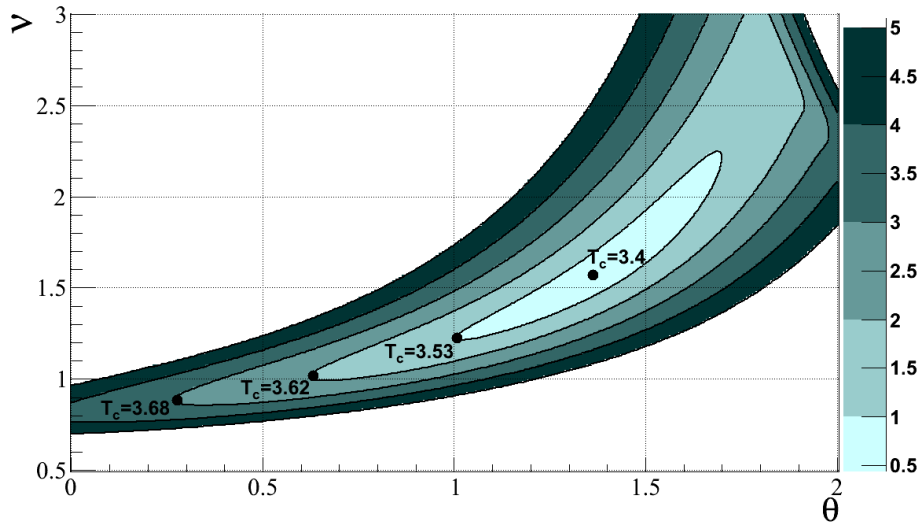

Figure 3. Scaling analysis for the RFIM. Shown are contours of $R_{\min}(\theta,\nu)$ in the plane of critical exponents (θ,ν); dots mark the critical temperature $T_{\rm c}$ at a few selected points, the best estimate being $T_{\rm c}\sim 3.4$. The plot shows a clear preference for the expected RFIM value $\theta\sim 1.5$, while $\theta=0$ of the pure Ising model, as well as $\theta=2$ of a first-order transition, are effectively excluded.

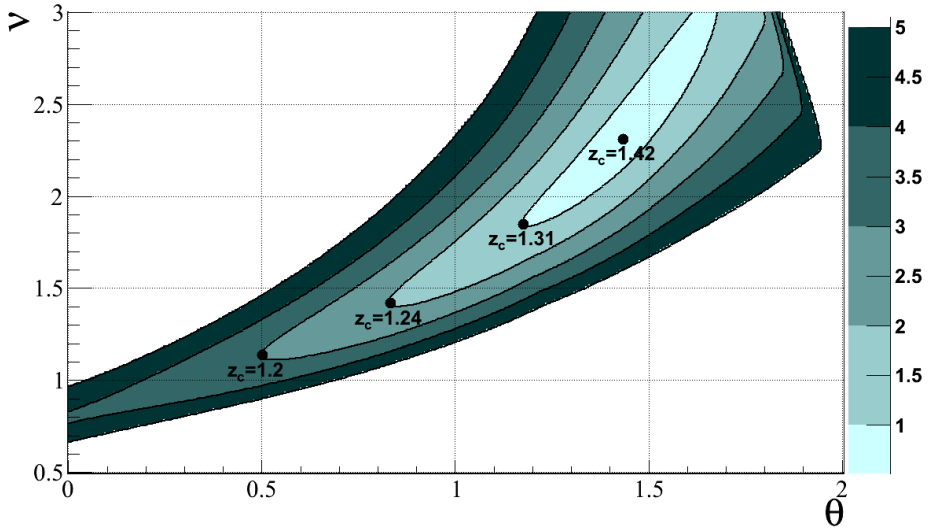

Figure 4. The analogue of Fig. 3 for the WR model with quenched obstacles; dots indicate the critical fugacity $z_{\rm c}$ at some selected points in the (θ,ν) plane. The global minimum of $R_{\min}(\theta,\nu)$ is at $z_{\rm c}\sim 1.42$, which thus serves as our best-estimate for the critical fugacity. As for the RFIM model, a clear preference for $\theta\sim 1.5$ is found, as well as the exclusion of $\theta=0$ and $\theta=2$.

3.2. WR model with quenched obstacles

The WR model [17] consists of unit-diameter spheres, of species A and B. The only interaction is a hard-core repulsion between particles of the opposite species. We consider the WR model in the presence of quenched obstacles; the spatial dimension is $d = 3$. The disorder configurations are generated by placing $0.02 \times L^d$ particles of species A, and the same number of species B, into a periodic cube of edge L (non-integer numbers are appropriately rounded to the next integer at random). The obstacles are inserted at random positions, irrespective of overlap between them, after which they remain quenched. Next, mobile particles are introduced and these interact with the quenched particles following the usual WR rule: quenched A-obstacles (B-obstacles) have a hard-core interaction with mobile B (A) particles. In this work, system sizes $L = 7, 8, \ldots, 12$ are used. For each system size, OPDs for $N \sim 10^4$ disorder configurations were generated at fugacities $z_A = z_B = 1.4$, which is the approximate location of the critical point as anticipated from our previous simulations [5]; all details regarding the simulation method can also be found in that reference.

To obtain ΔF_L via Eq. (13) over a range of z_B requires extracting the free energy barrier from several million(!) distributions, which obviously cannot be done by hand. To deal with the "problematic" distributions of Fig. 1(b) automatically, a numerical filter was therefore applied: if one of the two dominating peaks in the OPD is centered in the intermediate density range $0.20 z_B < \rho_A < 0.75 z_B$, the distribution is considered to not feature a distinct liquid and gas peak. For these distributions we set $\Delta F_{L,i} = 0$. Since for the values of z_B considered here no more than $\sim 0.1\%$ of the distributions failed this criterion, our results should not significantly depend on the filter. The results for $R_{\min}(\theta, \nu)$, as well as some estimates for the critical fugacity z_c obtained from minimizing R, are shown in Fig. 4. Note that, for the WR model, the analogue of Eq. (2) becomes $t := z_c/z_B - 1$. As in the RFIM, Fig. 4 features a clear preference for $\theta \sim 1.5$, and the competing values $\theta = 0$ and $\theta = 2$ of, respectively, the pure Ising model and a first-order transition, are effectively excluded. We interpret this finding as a strong sign that the WR model with quenched obstacles indeed belongs to the universality class of the RFIM. Note, however, that we cannot provide high-precision estimates of the critical exponents, nor of the critical "inverse temperature" z_c. There is a substantial range of possible values (θ, ν, z_c) in the region $R_{\min}(\theta, \nu) \leq 2$, i.e. the region where our results for the WR model and RFIM become quantitatively compatible.

3.3. Colloid-polymer mixtures in porous media

We now consider a colloid-polymer mixture confined to a porous medium. The colloids and polymers are unit-diameter spheres, with only a hard-core repulsion between colloid-colloid and colloid-polymer pairs (this is just the AO model [18, 19] with equally sized colloids and polymers). As porous medium we use a quenched configuration of polymers, which are distributed randomly in a periodic cube of edge L at the start of each simulation run (the average packing fraction of the quenched configuration $\eta_Q = 0.05$). The OPD for the AO model is the probability distribution $P_{L,i}(\eta_{\rm col}|z_{\rm col}, \eta_{\rm p}^{\rm r})$ [27], where i denotes the quenched polymer configuration for which the OPD was measured, $\eta_{\rm col}$ the colloid packing fraction, $z_{\rm col}$ the colloid fugacity, and $\eta_{\rm p}^{\rm r}$ the polymer reservoir packing fraction. Note that, for the AO model, $\eta_{\rm p}^{\rm r}$ is just the polymer fugacity multiplied by the volume of a single polymer, and thus

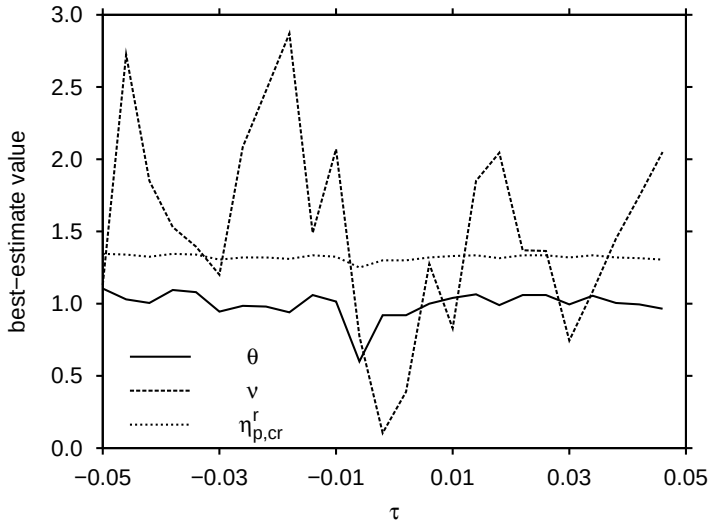

Figure 5. Best-estimates of $(\theta, \nu, \eta^{\rm r}_{\rm p,cr})$ versus the scaling variable τ for the AO model inside a porous medium; see details in text.

plays the role of inverse temperature. Consequently, the analogue of Eq. (2) becomes $t := \eta^{\rm r}_{\rm p}/\eta^{\rm r}_{\rm p,cr} - 1$. One of us (RV) recently studied the above model using the same type of quenched disorder. We now extend the analysis of that previous work [3] to the scaling of the free energy barrier.

One practical problem is that the number of disorder configurations in our AO data set is "only" $N \sim 10^3$, i.e. one order of magnitude below the value used in the analysis of the RFIM and WR model. Also the quality of individual distributions was worse compared to that of the latter two models. A further complication is that the AO model is asymmetric: the coexistence colloid fugacity is not trivially related to $\eta^{\rm r}_{\rm p}$. In contrast, for the WR model, it holds that $z_A = z_B$ at the critical point due to symmetry. Because of all these problems, the construction of contour plots, such as Fig. 3 and Fig. 4, was not feasible for the AO model, and so a modified analysis is presented. To this end, we extract the barrier ΔF_L from the quenched-averaged OPD, following the method outlined in the Appendix of Ref. [5]. This procedure yields a result similar to Eq. (13), but it is less susceptible to statistical uncertainties in individual distributions. Since the barrier is extracted from the quenched-averaged OPD, we loose information about the fluctuations between disorder configurations. In particular: Eq. (14) can no longer be used to calculate the typical statistical uncertainty $u(\tau)$ defined in Section 2.4. Hence, in the construction of the scaling plot $y_L(\tau)$, we cannot compare the deviation between the curves $\sigma(\tau)$ to the statistical uncertainty $u(\tau)$. Only best-estimates can be provided, which are obtained by minimizing the relative deviations between the curves. That is, for a given τ we minimize the value $\sigma(\tau)/y(\tau)$, where $y(\tau)$ is the average value of the $y_L(\tau)$. For $-0.05 < \tau < 0.05$, and system sizes $L = 10, 11, 12$ we computed these best-estimates: their variation with τ is shown in Fig. 5. If the collapse was perfect, the best-estimates should not depend on τ. Regarding $\eta^{\rm r}_{\rm p,cr}$ and θ this is confirmed, and from the average of the curves we conclude that $\eta^{\rm r}_{\rm p,cr} \sim 1.3$ and $\theta \sim 1.0$ for the AO model. However, it

is clear from Fig. 5 that no meaningful estimate of ν can be provided. We emphasize that $\eta^{\rm r}_{\rm p,cr} \sim 1.3$ deviates by about 10% from previous estimates. The reason is that, in Ref. [3], we assumed $\nu_{\rm RFIM} = 1.1$. However, from the analysis of the RFIM (Fig. 3) it transpires that $\nu_{\rm RFIM}$ may well be different. This is furthermore corroborated by the literature [14], where large variations in $\nu_{\rm RFIM}$ are also reported.

4. Conclusions

The aim of this paper was to test the relation $\Delta F_L \propto L^\theta$ in fluids with quenched disorder. This relation applies when the universality class is that of the RFIM [5]. For the WR and the AO model with quenched obstacles, our data confirm that ΔF_L diverges as a power law with system size at the critical point. This is an important qualitative indication that the universality class is no longer that of the pure Ising model, since then ΔF_L would be constant at criticality. For the WR model, θ is consistent with the RFIM value $\theta_{\rm RFIM} \sim 1.5$. For the AO model, $\theta \sim 1.0$ is found, which is somewhat below the RFIM value. Possible reasons for this discrepancy are (1) crossover effects [35] (in this case from pure Ising to RFIM universality), (2) corrections to scaling due to asymmetry, and (3) insufficient disorder averaging. We believe that the crossover scenario is the most likely explanation, since $\theta \sim 1.0$ is "in-between" the pure Ising value $\theta = 0$ and the RFIM value. Of course, all these problems could be solved by simulating larger systems and more disorder configurations, but the cost in CPU time is still prohibitively large. Our data also make clear that high-precision estimates of critical exponents and temperatures in random-field systems remain difficult to obtain in simulations. The data for the RFIM and the WR model reveal large variations, see Fig. 3 and Fig. 4, in particular for the correlation length critical exponent ν.

Acknowledgments

This work was supported by the *Deutsche Forschungsgemeinschaft* under the Emmy Noether program (VI 483/1-1).

References

[1] De Gennes PG, *Liquid-liquid demixing inside a rigid network: qualitative features*, J. Phys. Chem. **88**, 6469 (1984)
[2] Vink RLC, *Critical behavior of soft matter fluids in bulk and in random porous media: from Ising to random-field Ising universality*, Soft Matter **5**, 4388 (2009)
[3] Vink RLC, Binder K, and Löwen H, *Colloid-polymer mixtures in random porous media: finite size scaling and connected versus disconnected susceptibilities*, J. Phys.: Condens. Matter **20**, 404222 (2008)
[4] Vink RLC, Binder K, and Löwen H, *Critical Behavior of Colloid-Polymer Mixtures in Random Porous Media*, Phys. Rev. Lett. **97**, 230603 (2006)
[5] Vink RLC, Fischer T, and Binder K, *Finite size scaling in Ising-like systems with quenched random fields: Evidence of hyperscaling violation* (2010)
[6] Madden WG and Glandt ED, *Distribution functions for fluids in random media*, J. Stat. Phys. **51**, 537 (1988)
[7] De Sanctis Lucentini PG and Pellicane G, *Critical Behavior of Symmetrical Fluid Mixtures in Random Pores*, Phys. Rev. Lett. **101**, 246101 (2008)
[8] Parisi G, Picco M, and Sourlas N, *Scale invariance and self-averaging in disordered systems*, Europhys. Lett. **66**, 465 (2004)
[9] Wiseman S and Domany E, *Finite-Size Scaling and Lack of Self-Averaging in Critical Disordered Systems*, Phys. Rev. Lett. **81**, 22 (1998)

[10] Aharony A and Harris AB, *Absence of Self-Averaging and Universal Fluctuations in Random Systems near Critical Points*, Phys. Rev. Lett. **77**, 3700 (1996)
[11] Malakis A and Fytas NG, *Lack of self-averaging of the specific heat in the three-dimensional random-field Ising model*, Phys. Rev. E **73**, 016109 (2006)
[12] Wiseman S and Domany E, *Lack of self-averaging in critical disordered systems*, Phys. Rev. E **52**, 3469 (1995)
[13] Wiseman S and Domany E, *Self-averaging, distribution of pseudocritical temperatures, and finite size scaling in critical disordered systems*, Phys. Rev. E **58**, 2938 (1998)
[14] Nattermann T, *Theory of the Random Field Ising Model*, in: AP Young (Ed.), Spin Glasses and Random Fields, 277 (World Scientific, Singapore, 1998)
[15] Lee J and Kosterlitz JM, *New numerical method to study phase transitions*, Phys. Rev. Lett. **65**, 137 (1990)
[16] Binder K, *Finite size scaling analysis of ising model block distribution functions*, Z. Phys. B **43**, 119 (1981)
[17] Widom B and Rowlinson JS, *New Model for the Study of Liquid-Vapor Phase Transitions*, J. Chem. Phys. **52**, 1670 (1970)
[18] Asakura S and Oosawa F, *Surface Tension of High-Polymer Solutions*, J. Chem. Phys. **22**, 1255 (1954)
[19] Vrij A, *Polymers at Interfaces and the Interactions in Colloidal Dispersions*, Pure Appl. Chem. **48**, 471 (1976)
[20] Imbrie JZ, *Lower Critical Dimension of the Random-Field Ising Model*, Phys. Rev. Lett. **53**, 1747 (1984)
[21] Rieger H, *Critical behavior of the three-dimensional random-field Ising model: Two-exponent scaling and discontinuous transition*, Phys. Rev. B **52**, 6659 (1995)
[22] Newman MEJ and Barkema GT, *Monte Carlo study of the random-field Ising model*, Phys. Rev. E **53**, 393 (1996)
[23] Schwartz M, *The random-field puzzle. I. Solution by equivalent annealing*, J. Phys. C **18**, 135 (1985)
[24] Schwartz M, Gofman M, and Natterman T, *On the missing scaling relation in random field systems*, Physica A: Statistical Mechanics and its Applications **178**, 6 (1991)
[25] Gofman M, Adler J, Aharony A, Harris AB, and Schwartz M, *Evidence for two exponent scaling in the random field Ising model*, Phys. Rev. Lett. **71**, 1569 (1993)
[26] Frenkel D and Smit B, Understanding Molecular Simulation (Academic Press, San Diego, 2001)
[27] Vink RLC and Horbach J, *Grand canonical Monte Carlo simulation of a model colloid–polymer mixture: Coexistence line, critical behavior, and interfacial tension*, J. Chem. Phys. **121**, 3253 (2004)
[28] Orkoulas G, Fisher ME, and Panagiotopoulos AZ, *Precise simulation of criticality in asymmetric fluids*, Phys. Rev. E **63**, 051507 (2001)
[29] Borgs C and Kappler S, *Equal weight versus equal height: a numerical study of an asymmetric first-order transition*, Phys. Lett. A **171**, 37 (1992)
[30] Binder K, *Monte Carlo calculation of the surface tension for two- and three-dimensional lattice-gas models*, Phys. Rev. A **25**, 1699 (1982)
[31] Ferrenberg AM and Swendsen RH, *New Monte Carlo technique for studying phase transitions*, Phys. Rev. Lett. **61**, 2635 (1988)
[32] Binder K and Heermann DW, Monte Carlo Simulation in Statistical Physics: An Introduction (Springer, Berlin, Germany, 2002)
[33] Newman MEJ and Barkema GT, Monte Carlo Methods in Statistical Physics (Clarendon Press, Oxford, 1999)
[34] Zinn-Justin J, *Precise determination of critical exponents and equation of state by field theory methods*, Phys. Rep. **344**, 159 (2001)
[35] Kim YC, Anisimov MA, Sengers JV, and Luijten E, *Crossover Critical Behavior in the Three-Dimensional Ising Model*, J. Stat. Phys. **110**, 591 (2003)